Supplementary Information

Steric effect of CN vacancy for boosting CO_2 electroreduction to CO with ultrahigh selectivity

Qiang Zhang[*a], Jianlin Wang[a], Fang Guo[a], Yang Zhou[b], Ge He[*c], Junqiang Xu[*a]

a School of Chemistry & Chemical Engineering, Chongqing University of Technology, Chongqing 400054, P. R. China.

b the Analytical and Testing Center, Chongqing University, Chongqing 400044, P. R. China.

c College of Biomass Science and Engineering, Sichuan University, Chengdu 610065, China.

**Corresponding authors: School of Chemistry & Chemical Engineering, Chongqing University of Technology, Chongqing 400054, P. R. China.*

E-mail addresses: zqiang@cqut.edu.cn (Qiang Zhang); hege@scu.edu.cn (Ge He); xujunqiang@cqut.edu.cn (Junqiang Xu)

Mailing address for correspondence:

Dr. Zhang, Qiang (Prof.)

School of Chemistry & Chemical Engineering, Chongqing University of Technology, No.66 Hongguang Rd., Banan, Chongqing 400054, China

Tel: +86-23-625678923

Fax: +86-23-625678923

E-mail: zqiang@cqut.edu.cn

1. Experimental

1.1. Catalyst synthesis and cold H_2-plasma bombardment

Solution A:1.32 g Trisodium citrate and 0.87 g Cobaltous Nitrate Hexahydrate were weighed into a clean beaker and dissolved in 100 ml deionized water. Solution B: add 0.66 g potassium hexacyanocobaltate (III) to another beaker, then add 100 ml deionized water and stir until clarified. First, solution A and solution B were mixed at room temperature and stirred 30 min to obtain a clarified solution. Then, the obtained solution was aged at room temperature for 24 hours to make it crystallize. Finally, the obtained crystalline material was filtered and washed, and then dried in an oven at 70°C to obtain Co PBA (Co Prussian blue analogue). Then, the Co PBA precursor was activated by OPS Plasma (SY-DT02) at 400 mTorr H_2 pressure and 100 W power for 10-50 min, and the Co PBA-V_{CN} catalyst was obtained.

1.2. Characterization

The crystal structure of the samples was characterized by XRD diffractometer (equipped with graphite Monochromator, Rigaku D/max-3C) under Cu Kα (40 kV, 40 mA, λ= 1.542 Å). The morphology of the sample was observed by TEM and SEM, and the element distribution of the sample was obtained by EDX. The morphology of the sample was observed by Transmission Electron Microscopy (FEI Talos F200s G2) and Scanning Electron Microscopy (JSM-7800F), and the element distribution of the sample was obtained by energy dispersive X-ray spectroscopy（EDX）. The crystal cell structure of the sample was analyzed by High-resolution Transmission Electron Microscopy (JEM-2100F) and High-angle annular dark-field. The X-ray photoelectron spectroscopy (ESCALAB250Xi) of the sample was recorded by using a monochromatic Al-Kα X-ray source (1486.6 eV) with a voltage of 15KV and a current of 30 mA as the excitation source, and then the valence state of the elements in the sample was analyzed. The Raman spectrum and in-situ Raman spectrum of the sample was recorded by laser Raman spectrometer (HR Evolution). The coordination and defects

of the samples were analyzed by electron paramagnetic resonance spectrometer (EMXplus-9.5/12) and positron annihilation lifetime spectrometer (DPLS3000).

1.3. Electrochemical measurements

CO_2RR was carried out in a standard three-electrode system using 0.1m potassium bicarbonate solution (298 K, pH=6.8) as electrolyte in an airtight two-chamber electrochemical cell (Nafion-212 membrane separation). The counter electrode used in the experiment was platinum electrode, the reference electrode was calomel electrode, the working electrode was glassy carbon electrode and the electrochemical workstation was CHI-660E. First, the catalyst, isopropanol and Nafion solution (5 wt.%, Dupont) were mixed and then the mixture was treated by ultrasonic to obtain the catalyst slurry. Then the slurry was coated on the glassy carbon electrode and air-dried to remove the solution to get the working electrode. The electrolyte was purged by high-purity argon (99.999%) for half an hour to remove the impurity gas, and then high purity CO_2 (99.99%) was injected into the electrolyte to form a saturated CO_2 solution. The catalytic activity of the catalyst was evaluated by cyclic voltammetry (CV) and linear sweep voltammetry (LSV). The stability of the catalyst was analyzed by chronoamperometry. The electrochemical impedance of the catalyst was analyzed by electrochemical impedance spectroscopy (frequency 1-10^5 Hz, potential -0.9 V *vs.* RHE, amplitude 5mV).

The gaseous products were detected by gas chromatograph (SC-3000B) with TDX01 molecular sieve column every 30 minutes. The composition of liquid sample was analyzed by nuclear magnetic resonance spectroscopy, and the result was shown in figure S6. Nuclear magnetic resonance sample preparation: 0.1ml D_2O containing 0.05 ml dimethyl sulfoxide was used as the internal standard liquid. After the electrolytic reaction, the electrolyte of 0.1ml was mixed with the internal standard solution for NMR detection. Faraday efficiency and conversion frequency are calculated by measuring the product and current value of the reaction at constant potential for 5 h.

The gaseous products were analyzed every 30 min by online gas chromatography (SC-3000B) equipped with a TCD detector and a columns of molecular sieve TDX01. The liquid products were determined using ^{1}H nuclear magnetic resonance spectroscopy (NMR, Bruker 500 UltraShield^{TM}), and the results are shown in Fig. S6. Typically, 0.1 mL of $KHCO_3$ solution after electrolysis was mixed with 0.1 mL of D_2O containing 0.05 mL of DMSO as an internal standard. The reported faradaic efficiency (FE) and turnover frequency (TOF) were calculated on the basis of product distribution and current values after a 5 h reaction at constant potentials.

In all measurements, we used SCE as the reference electrode. For comparison with the literature, all the potentials in this paper were converted to the RHE reference:

$$E(vs.\ RHE) = E(vs.SCE)+0.24\ V+0.059*pH$$

CO_2RR was conducted in CO_2-saturated 0.1 M $KHCO_3$ solution (pH 6.8) at room temperature and atmospheric pressure.

Faradaic efficiency (FE) of gaseous products at each applied potential was calculated based on the equation:

$$FE = \frac{z \cdot P \cdot F \cdot V \cdot v_i}{R \cdot T \cdot J}$$

Partial current density for formate normalized by the geometrical electrode area (J_{formate}, A cm^{-2}) was determined by calculating the total current density multiplied by FE of formate:

$$J_{formate} = FE_{formate} \cdot J$$

Formate mass activity was determined by formate partial current density divided by catalyst mass on the electrode:

$$Mass\ activity = \frac{J_{formate}}{m}$$

Formate production rate normalized by the geometrical electrode area (n, mol·cm^{-2}·h^{-1}) was calculated based on the formula:

$$n = \frac{P \cdot V \cdot v_i}{R \cdot T} \times 3600$$

Turnover Frequency (TOF, h^{-1}) for formate production per metal site is defined as the mole of formate product formed divided by the mole of Co metals in catalysts employed in the CO_2 electrolysis per hour, which can be obtained by following formula:

$$TOF = \frac{n \cdot M}{m \cdot \omega}$$

Where z is the number of electrons transferred per mole of gas product (z is 4 for formate), F is Faraday constant (96500 $C \cdot mol^{-1}$), P is pressure (1.01×10^5 Pa), V is the gas volumetric flow rate (3.33×10^{-7} $m^3 \cdot s^{-1}$), v_i is the volume concentration of gas product determined by GC, T is the temperature (298.15 K), R is the gas constant (8.314 J $mol^{-1} \cdot K^{-1}$), J is the steady-state current at each applied potential (A), m is the catalyst mass on the electrode ($g \cdot cm^{-2}$), ω is the mass percentage of Co metal in the catalysts detected by EDS, and M is atomic mass of metal ($g \cdot mol^{-1}$).

To evaluate the effect of surface area, we measured the electrochemically active surface area (ECSA) for different catalysts electrodes from the electrochemical double-layer capacitance of the catalytic surface [1]. The electrochemical capacitance was determined by measuring the non-Faradaic capacitive current associated with double-layer charging from the scan-rate dependence of cyclic voltammograms (CVs). The double-layer charging current is equal to the product of the scan rate, v, and the electrochemical double-layer capacitance, C_{DL}, as given by the equation:

$$i_c = vC_{DL}$$

Thus, a plot of i_c as a function of v yields a straight line with a slope equal to C_{DL}. The specific ECSA of the electrodes is calculated from the double layer capacitance according to the equation:

$$\text{ECSA} = C_{DL}/C_s$$

Where C_s is the specific capacitance of the sample or the capacitance of an atomically smooth planar surface of the material per unit area under identical electrolyte conditions. For

our estimates of surface area, we use general specific capacitances of Cs = 0.020 mF based on typical reported values.

1.4. Product Analysis

The gaseous products were detected by gas chromatograph (SC-3000B) with TDX01 molecular sieve column every 30 minutes. The composition of liquid sample was analyzed by nuclear magnetic resonance spectroscopy, and the result was shown in **Fig. S6**. Nuclear magnetic resonance sample preparation: 0.1ml D_2O containing 0.05 ml dimethyl sulfoxide was used as the internal standard liquid. After the electrolytic reaction, the electrolyte of 0.1ml was mixed with the internal standard solution for NMR detection. Faraday efficiency and conversion frequency are calculated by measuring the product and current value of the reaction at constant potential for 5 h.

1.5. In situ ATA-SEIRAS characterization

Pt foil, and SCE electrode were served as counter electrode and reference electrode. Electrocatalysts suspension were dropped on silicon substrate covered with gold film via magnetron sputtering device to form the working electrode. A H-type electrochemical cell with Nafion membrane separation was designed to accommodate the Si prism and to avoid any possible cross-contamination. A IRT racer100 (Shimadzu, Japan) spectrometer equipped with a liquid nitrogen-cooled MCT detector were employed for the electrochemical ATR-SEIRAS. Before performing experiment, the infrared analysis was monitored on the background was measured in 0.1M $KHCO_3$ CO_2-satuated solution. Adjust the constant potential of reaction work from -0.16 V to -1.16 V vs. RHE to generate intermediates, and keep each potential for 2 minutes.

1.6. Density functional theory calculations

The Cambridge Sequential Total Energy Package (CASTEP) based on pseudopotential plane wave (PPW) method was used for density functional theory (DFT) calculation. The ultrasoft (USP) potentials was used to describe the electron-ion interaction. The wave function

was expanded by the plane wave basis set and the cutoff kinetic energy was 400 eV. the functional parametrized by Perdew-Burke-Ernzerhof (PBE), a form of the general gradient approximation (GGA) was used to describe the electron-electron relationship. The DFT-D2 method proposed by Grimme was used to describe the Vander Waals interaction.

The positions of all atoms are allowed to relax in the process of geometric optimization. The Monkhorst-Pack (MP) grid of special points was used to calculate the Brillouin zone integral. The model cell was A (2×2×2) k-point grid. The convergence criterion for the electronic self-consistent field (SCF) loop was set to 1×10^{-6} eV/atom. The residual force of the atomic structure was optimized to below 0.03 eV. The finite basis correction method was used to optimize the cell parameters until the stress was less than 0.05 GPa.

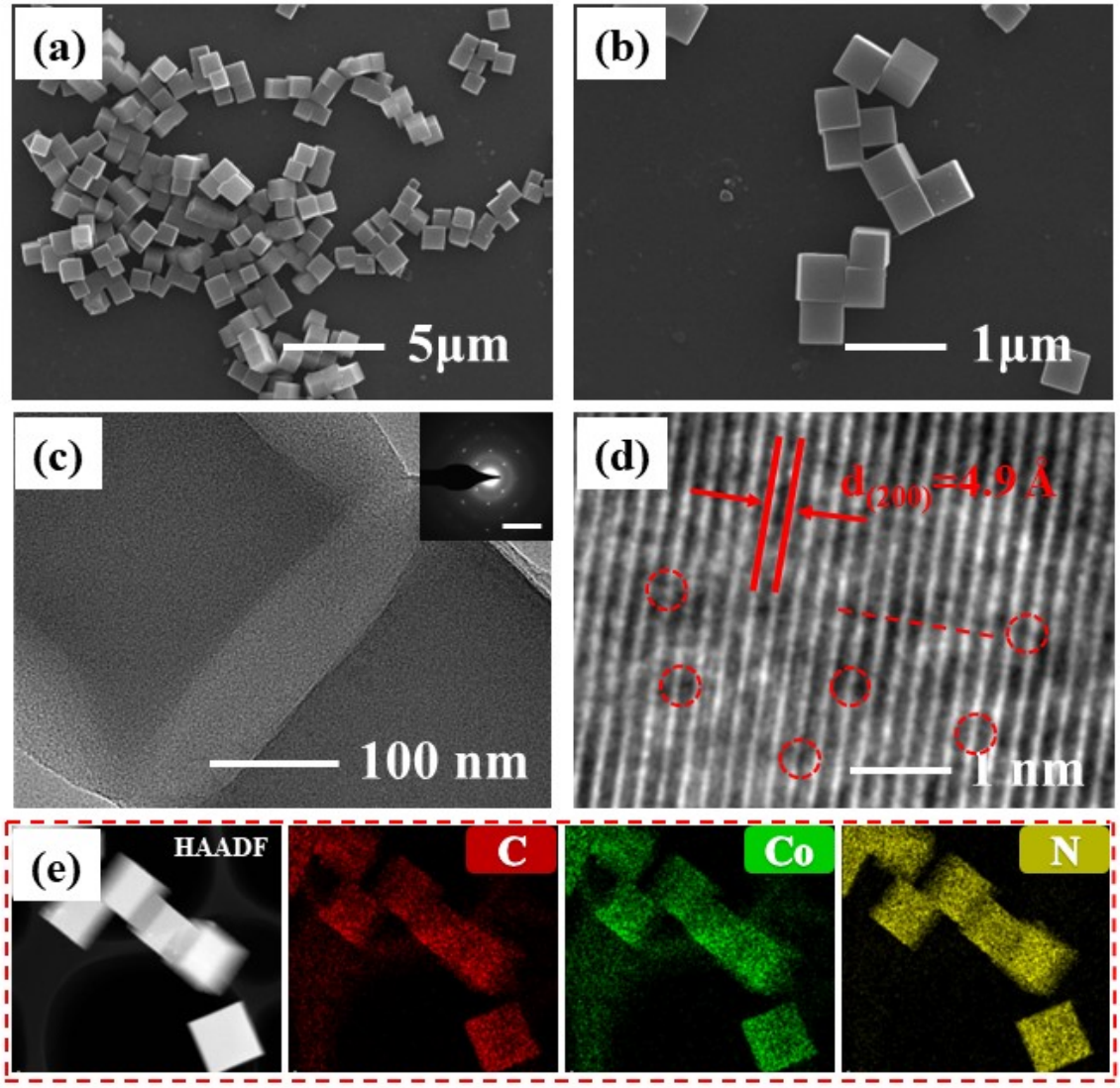

Fig. S1. (a-b) SEM image of Co PBA-V_{CN}. (c) TEM image of Co PBA-V_{CN}. (d) HRTEM image of Co PBA-V_{CN} (inset shows enlarged HRTEM images). (e) TEM-EDS mapping of Co PBA-V_{CN}.

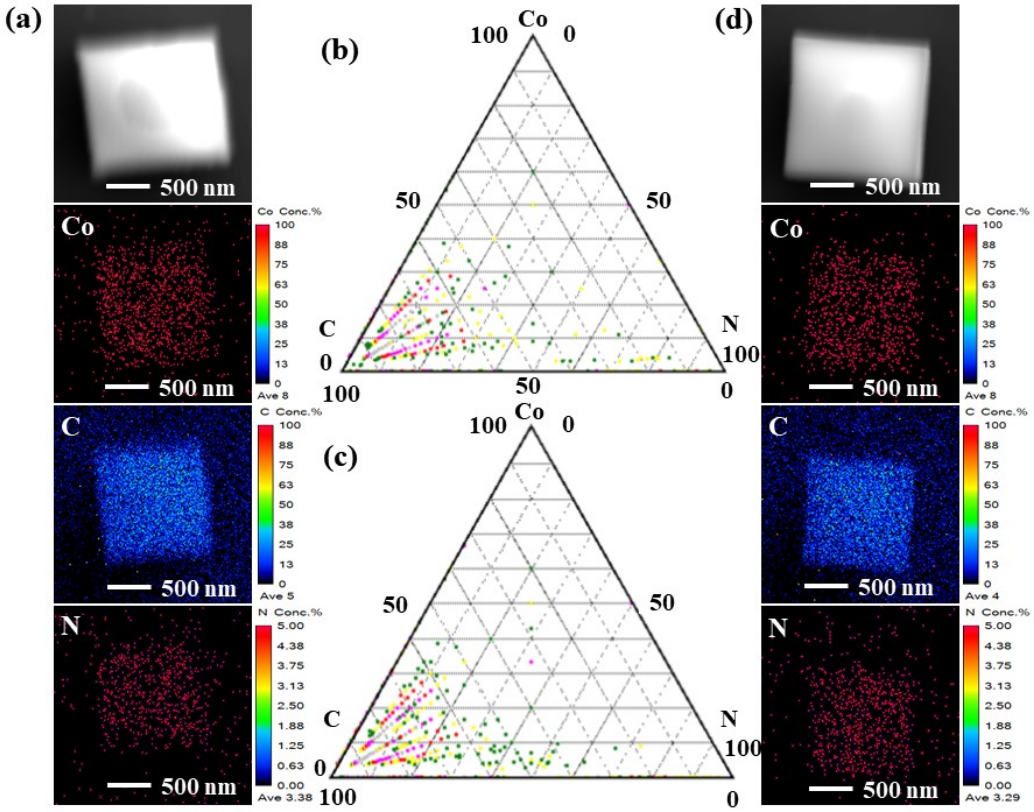

Fig. S2. EPMA analysis and elemental mapping of Co PBA (a) and Co PBA-V_{CN} (d). Three phase diagram of element statistics of Co PBA (b) and Co PBA-V_{CN} (c).

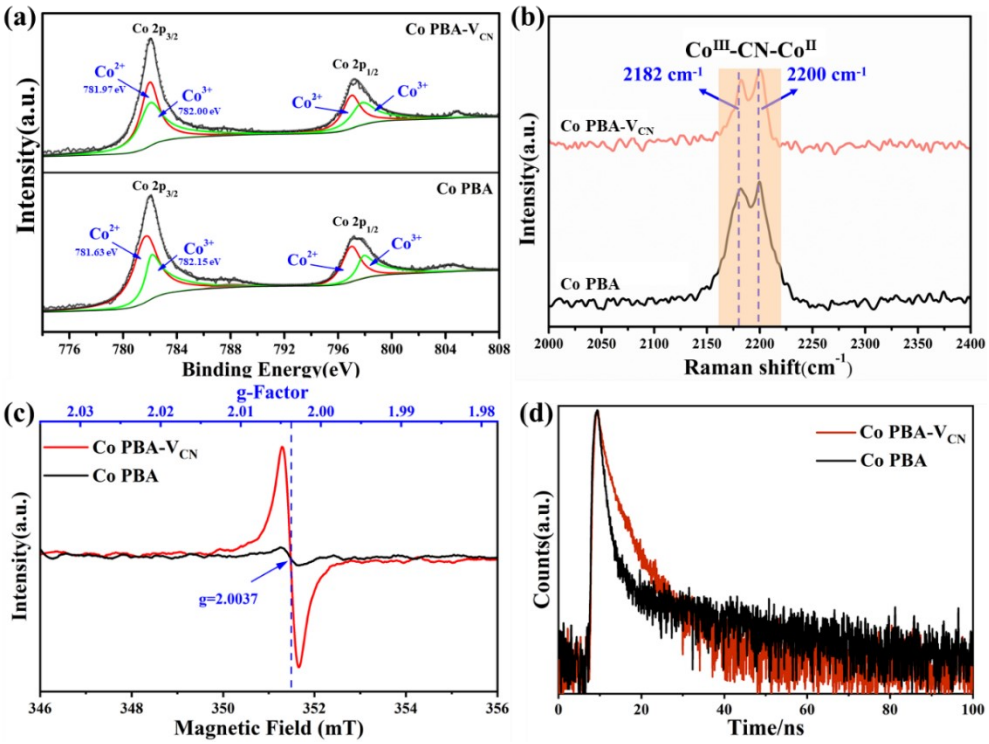

Fig. S3. Spectroscopic evidence of plasma-induced formation of C vacancies. (a) Co 2p XPS spectra of Co PBA, Co PBA-V_{CN} and Co PBA-pyrolysis. (b) Raman spectra of Co PBA, Co PBA-V_{CN} and Co PBA-pyrolysis. (c) ESR spectra of Co PBA and Co PBA-V_{CN}. (d) PAS analysis of Co PBA and Co PBA-V_{CN}.

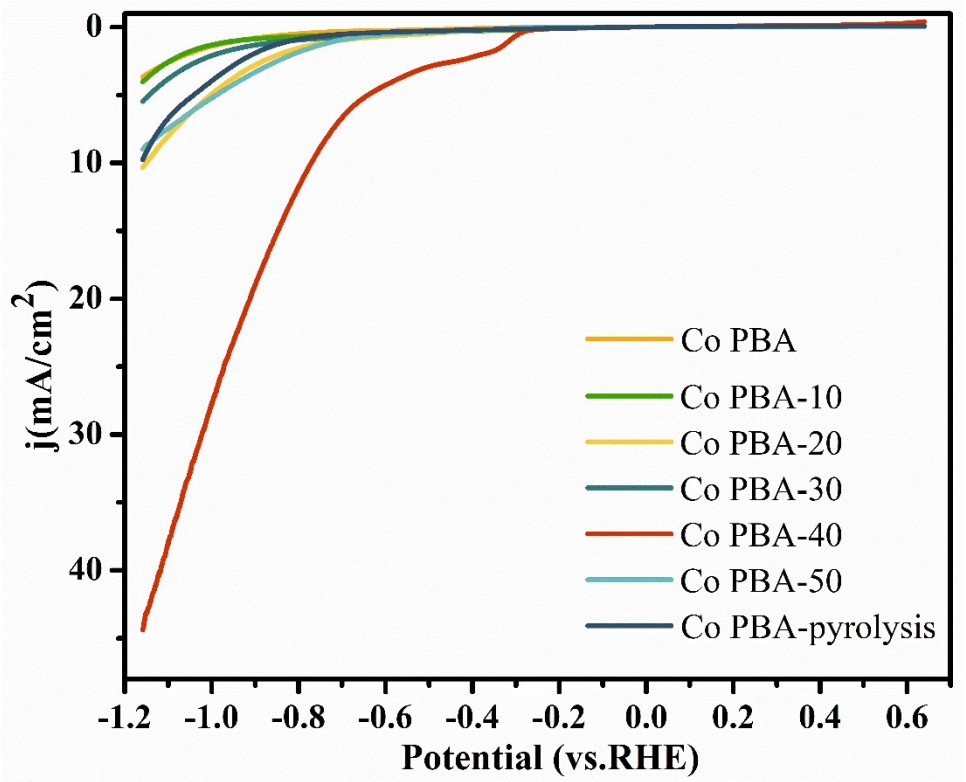

Fig. S4. The LSV curves of different catalysts with CO_2 in 0.1 M $KHCO_3$.

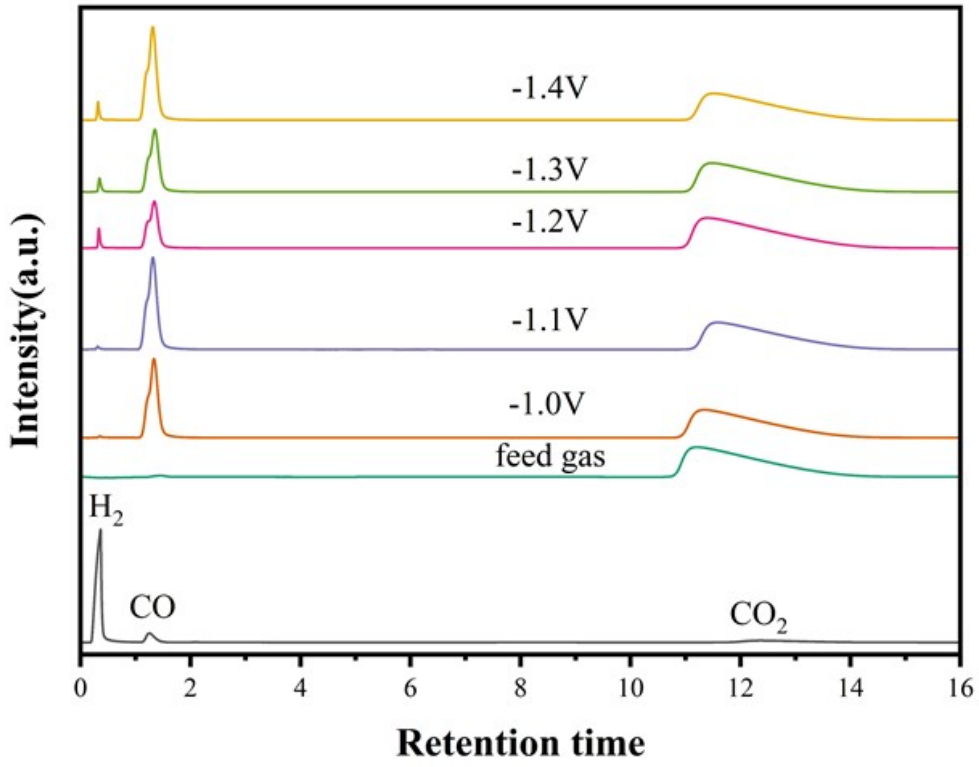

Fig. S5. Gas chromatography spectra of the gas products of CO_2 electrochemical reduction over Co PBA-V_{CN} at different potentials.

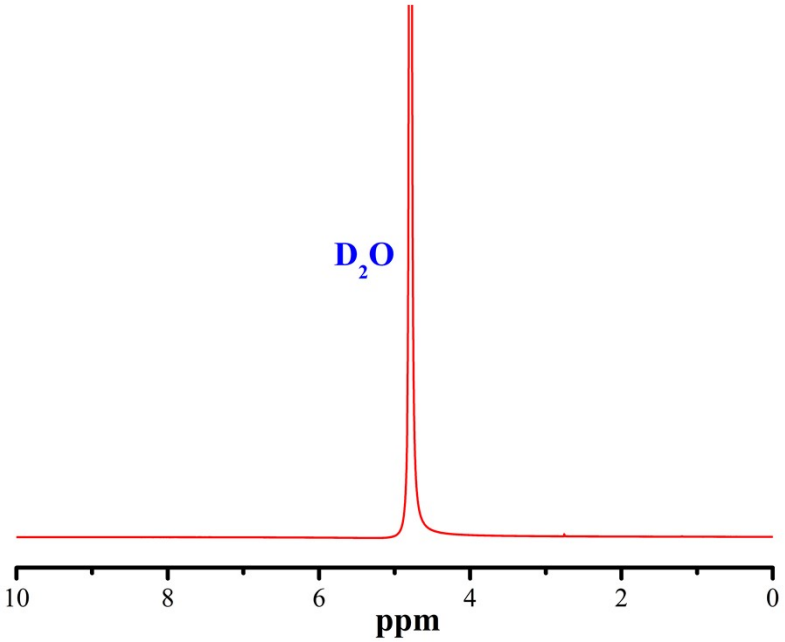

Fig. S6. ^{1}H-NMR spectra of the liquid products of CO_2 electrochemical reduction over Co PBA-V_{CN} at -0.9 V vs. RHE for 5 h.

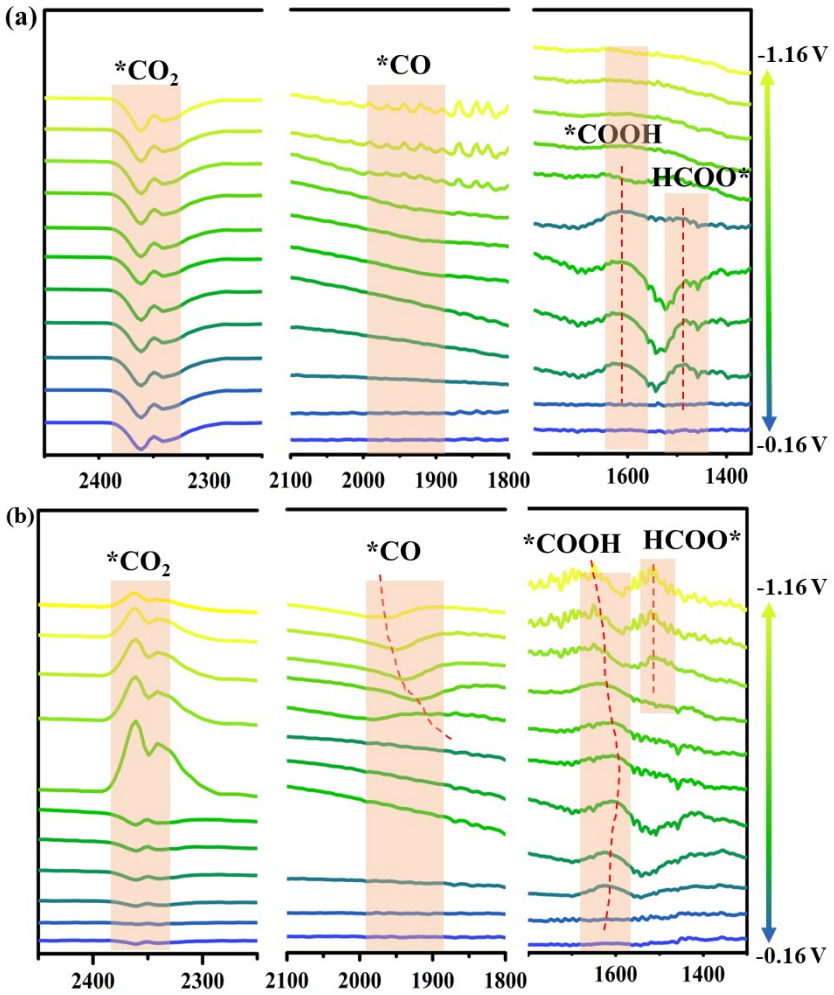

Fig. S7. In situ ATR-SEIRAS characterization for key intermediates against different potential (-0.16 ~ -1.16 V vs. RHE) over (a) Co PBA and (b) Co PBA-V_{CN}.

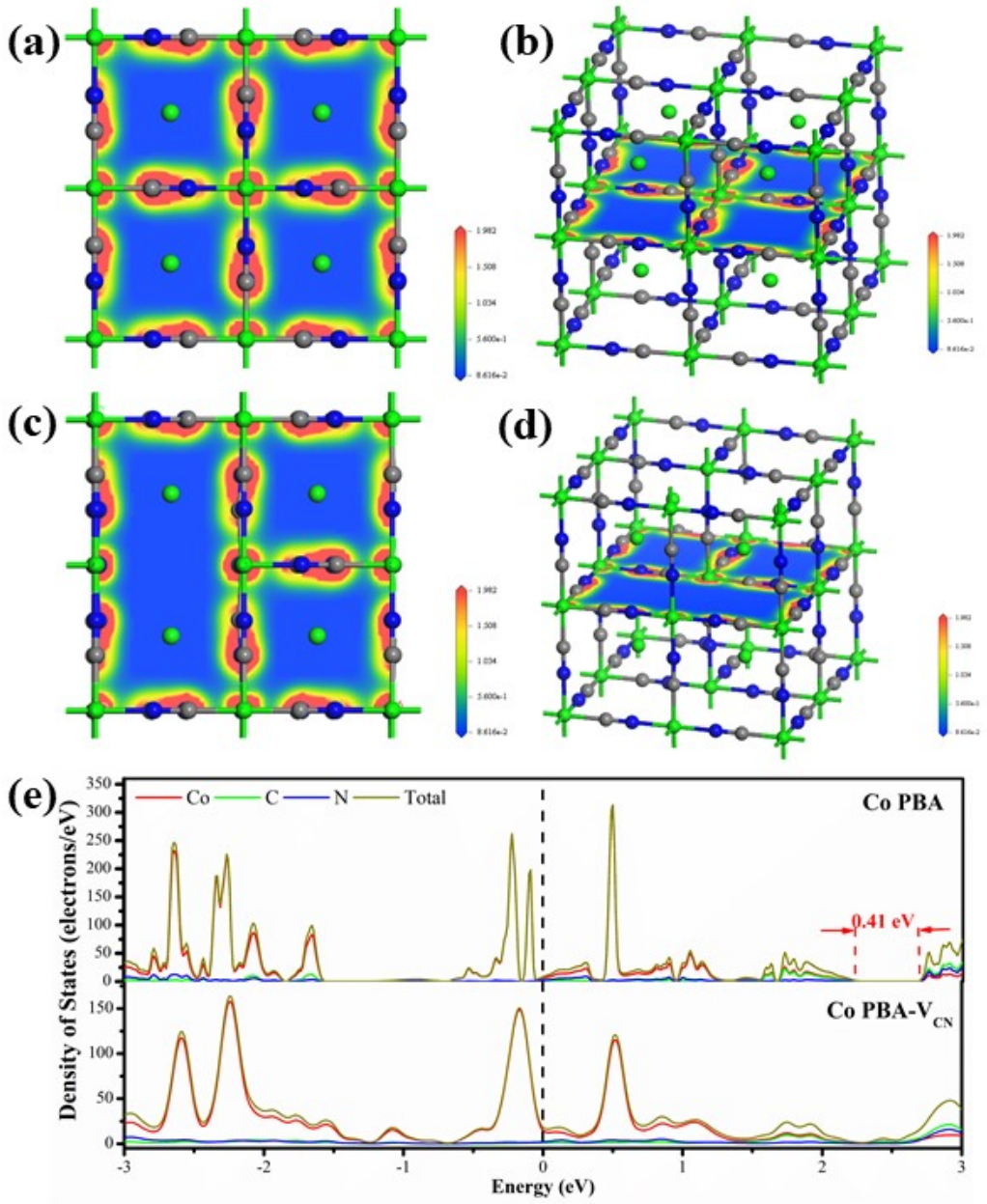

Fig. S8. (a-b) Electron density contour maps of Co atom in Co PBA. (c-d) Electron density contour maps of Co atom in Co PBA-V_{CN}. (e) Calculated partial density of states of Co PBA and Co PBA-V_{CN}.

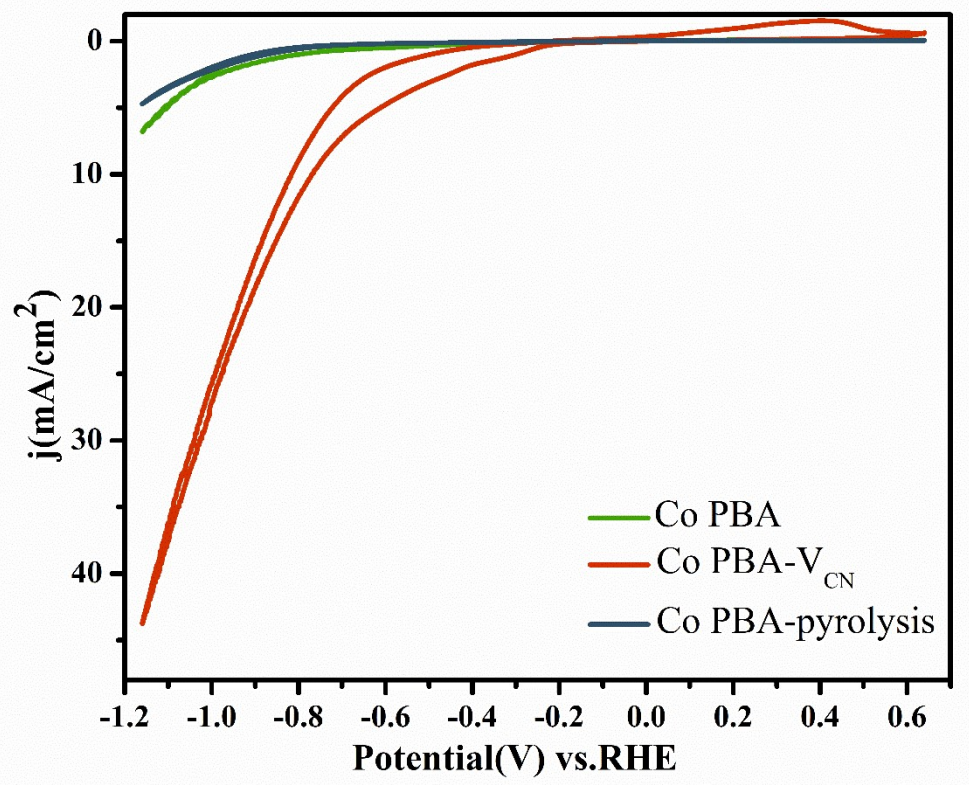

Fig. S9. CV curve of Co PBA, Co PBA-V_{CN} and Co PBA-pyrolysis electrodes in 0.1 M $KHCO_3$ saturated with CO_2.

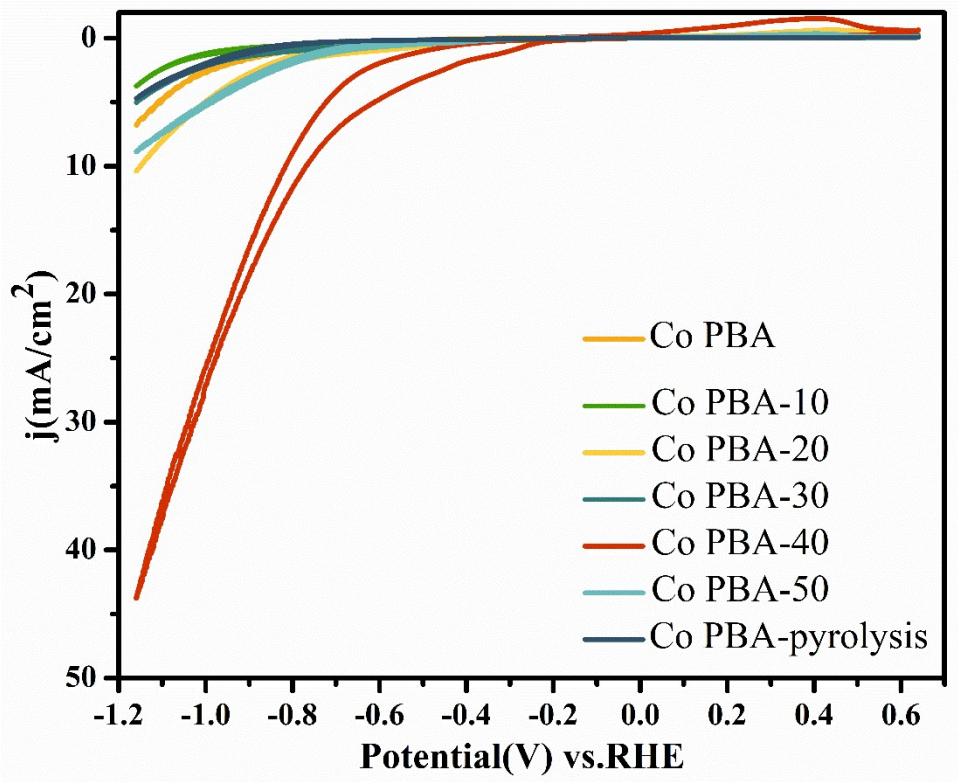

Fig. S10. CV curve of different catalysts electrodes in 0.1 M $KHCO_3$ saturated with CO_2.

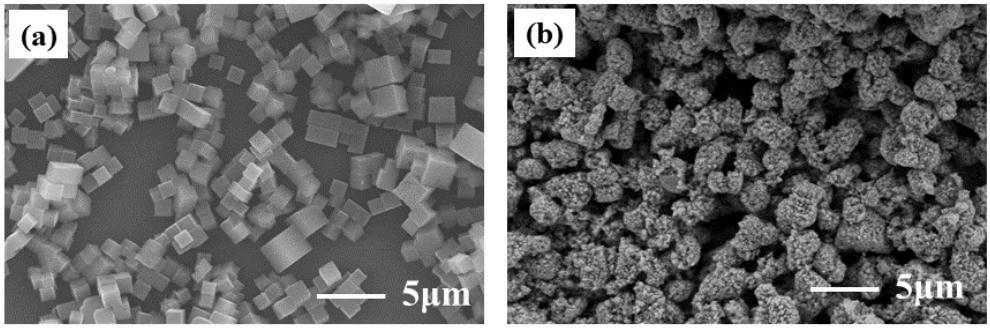

Fig. S11. (a) SEM image of Co PBA and Co PBA-pyrolysis.

Table S1 Summery of representative reports on CO generation through CO_2RR in aqueous solutions.

Catalysts	Work potential	CO faradaic efficiency	Stability	Overpotential at 5.6 mA/cm^2	Onset potential	Ref.
Co PBA-V_{CN}	-0.9 V	~100%	87 h	0.16 V Vs. RHE	-0.28 V Vs. RHE	This work
ZIF-8 derived Ni SAs/N-C	-0.9 V	71.9%	60 h	0.30 V Vs. RHE	-0.57 V Vs. RHE	S1
Ni-N3-C.	-0.65 V	95.6%	10 h	0.17 V Vs. RHE	-0.45 V Vs. RHE	S2
R-ZnO/rGO	-1.0 V	94.3%	21 h	0.5 V Vs. RHE	-0.75 V Vs. RHE	S3
ZIF-A-LD	-1.1 V	90.57%	10 h	0.5 V Vs. RHE	-0.75 V Vs. RHE	S4
CoPc/CNT	-0.63 V	92%	10 h	0.06 V Vs. RHE	-0.36 V Vs. RHE	S5
Ni-N/PC-900	-0.8 V	96.5%	73 h	0.31 V Vs. RHE	-0.21 V Vs. RHE	S6
Fe^{3+}–N–C	-0.45 V	90%	12 h	0.12 V Vs. RHE	-0.19 V Vs. RHE	S7
Au needles	-0.35 V	95%	8 h	/	-0.35 V Vs. RHE	S8
Ni@NiNCM	-0.9 V	97.6%	10 h	0.26 V Vs. RHE	-0.35 V Vs. RHE	S9

References

S1 C. Zhao, X. Dai, T. Yao, W. Chen, X. Wang, J. Wang, J. Yang, S. Wei, Y. Wu, Y. Li, *J. Am. Chem. Soc.*, 2017, **139**: 8078-8081.

S2 Y. Zhang, L. Jiao, W. Yang, C. Xie, H.L. Jiang, *Angew. Chem. Int. Ed.*, 2021, **60**, 7607-7611.

S3 D.L.T. Nguyen, C.W. Lee, J. Na, M.-C. Kim, N.D.K. Tu, S.Y. Lee, Y.J. Sa, D.H. Won, H.-S. Oh, H. Kim, B.K. Min, S.S. Han, U. Lee, Y.J. Hwang, *ACS Catal.*, 2020, **10**: 3222-3231.

S4 S. Dou, J. Song, S. Xi, Y. Du, J. Wang, Z.F. Huang, Z.J. Xu, X. Wang, *Angew. Chem. Int. Ed.*, 2019, **58**: 4041-4045.

S5 X. Zhang, Z. Wu, X. Zhang, L. Li, Y. Li, H. Xu, X. Li, X. Yu, Z. Zhang, Y. Liang, H. Wang, *Nat. Commun.*, 2017, **8**: 14675.

S6 W. Hua, H. Sun, L. Lin, Q.Q. Mu, B.Y. Yang, Y.H. Su, H.R. Wu, F.L. Lyu, J. Zhong, Z. Deng, Y. Peng, *Chem. Eng. J.*, 2022, **446**: 137296.

S7 J. Gu, C.S. Hsu, L. Bai, H.M. Chen, X. Hu, *Science*, 2019, **364(6445)**: 1091-1094.

S8 M. Liu, Y. Pang, B. Zhang, P. De Luna, O. Voznyy, J. Xu, X. Zheng, C.T. Dinh, F. Fan, C. Cao, F.P. de Arquer, T.S. Safaei, A. Mepham, A. Klinkova, E. Kumacheva, T. Filleter, D. Sinton, S.O. Kelley, E.H. Sargent, *Nature*, 2016, **537(7620)**: 382-386.

S9 X. Wang, X. Sang, C.L. Dong, S. Yao, L. Shuai, J. Lu, B. Yang, Z. Li, L. Lei, M. Qiu, L. Dai, Y. Hou, *Angew. Chem., Int. Ed. Engl.*, 2021, **60(21)**: 11959-11965.